TECHNICAL MEMORANDUM

698

Large-scale distinctions between MJO and non-MJO convective initiation over the tropical Indian Ocean

Jian Ling[1,2], Chidong Zhang[2] and Peter Bechtold[1]

Research Department

May 2013

To be published in *Journal of the Atmospheric Sciences*

[1] ECMWF

[2] RSMAS, University of Miami

European Centre for Medium-Range Weather Forecasts
Europäisches Zentrum für mittelfristige Wettervorhersage
Centre européen pour les prévisions météorologiques à moyen

Series: ECMWF Technical Memoranda

A full list of ECMWF Publications can be found on our web site under:
http://www.ecmwf.int/publications/

Contact: library@ecmwf.int

European Centre for Medium Range Weather Forecasts
Shinfield Park, Reading, Berkshire RG2 9AX, England

Abstract

In this study, we seek large-scale signals that may distinguish MJO from non-MJO convective events before they start over the Indian Ocean. We found three such signals. Low-level easterly anomalies extend from the surface to the mid troposphere and move from the western to eastern Indian Ocean. Surface pressure anomalies exhibit a zonal structure of wavenumber one with an equatorial low pressure surge penetrating eastward from Africa through the Indian Ocean and reaching the Maritime Continent. Negative temperature anomalies in the mid-upper troposphere start over the Indian Ocean and move eastward. All of them emerge 20 days before convective initiation of the MJO and move eastward at speeds close to that of the MJO without any direct connection to MJO convection. They are not obviously related to the extratropics in any discernible way or any preceding MJO events. They are absent in non-MJO convective events. These signals provide useful information for forecasting MJO initiation over the Indian Ocean. They can be signatures of a dry dynamics mode of the MJO, if it exists.

1 Introduction

Convective initiation is perhaps the most understudied and least understood aspect of the Madden-Julian Oscillation (MJO, Madden and Julian 1971, 1972). MJO prediction by some models suffers from particularly low skill at MJO initiation (Seo et al. 2009; Kim et al. 2010). As summarized in Zhang (2005), possible mechanisms for MJO initiation include continuation and amplification of a preexisting event (Knutson et al. 1986; Knutson and Weickmann 1987), extratropical influences (Lau and Peng 1987; Frederiksen and Frederiksen 1997; Hsu et al. 1990; Lin et al. 2007; Ray et al 2009; Ray and Zhang 2010), local energy discharge-recharge processes (Hendon 1988; Blade and Hartmann 1993; Kemball-Cook and Weare 2001), and convective stochastic forcing (Neelin and Yu 1994; Yu and Neelin 1994).

Initiation of the MJO has drawn more research attentions lately. Matthews (2008) classified the MJO events into two types: the successive MJO, which immediately follows a preceding MJO event, and the primary MJO, which starts without any immediate preceding MJO event. He found that 40% of total MJO events are primary. Most variables relevant to the MJO, such as humidity and boundary layer convergence, show no evident signal during initiation of the primary MJO; they only become significant once the MJO is generated. Webber et al. (2012) proposed that initiation of the primary MJO can be related to westward propagation of a downwelling oceanic Rossby wave. Straub (2012) found that slowly eastward-propagating 850 hPa easterly anomalies over the Indian Ocean precede initiation of the primary MJO by at least 10 days. Seo and Kumar (2008) and Zhao et al (2013) suggested that low-level moisture convergence plays a key role in MJO initiation. Zhang and Ling (2012) documented the structure and evolution of potential vorticity (PV) through convective initiation to mature stages of the MJO over the tropical Indian Ocean. The MJO PV structure cannot be explained by eastward PV advection from Africa; it is locally generated by MJO and stochastic convection over the Indian Ocean. Seo and Song (2012) showed that the mid-tropospheric PV anomaly acts as a dynamic forcing and plays an important role in the initiation of boreal summer intra-seasonal oscillation.

Most, if not all, previous studies on MJO initiation focused on the MJO alone. In fact, there are two issues related to convective initiation of the MJO. One is when, where and how active convection may occur in a large area over the tropical Indian Ocean. The other one is whether such a large-scale convective activity would lead to an MJO event. All large-scale convective events over the tropical

Indian Ocean do not lead to the MJO. We cannot fully understand MJO convective initiation until we know why some large-scale convective events become the MJO while others do not.

This study seeks signals that may distinguish large-scale convective events over the tropical Indian Ocean that lead to the MJO from those that do not. We anticipate that MJO and non-MJO convective events may share common features. We are particularly interested in possible precursors in large-scale fields prior to the convective initiation of the MJO that are missing in non-MJO convective events. Such signals must be identified when MJO and non-MJO convective events are directly compared.

We first defined convective initiation over the tropical Indian Ocean and identified MJO and non-MJO events (section 3) using satellite and reanalysis data (section 2). Then we compared composites of MJO and non-MJO events, with an emphasis on time prior to their convective initiation (section 4). We choose to examine precipitation, low-level zonal wind, surface pressure, tropospheric temperature, moisture, diabatic heating, potential vorticity, sea surface temperature, and gross moist stability. A summary and discussions are given in section 5.

2 Data and method

The following data were used in this study over the period of 1998-2009:

a) Daily rainfall data (0.25° x 0.25°) from the Tropical Rainfall Measuring Mission (TRMM, Kummerow et al. 2000) Multi-satellite Precipitation Analyisis (Huffman et al. 2007). They were used to identify large-scale convective events over the tropical Indian Ocean and to classify them into different categories (MJO vs. non-MJO events).

a) The all-season real-time multivariate MJO (RMM) index of Wheeler and Hendon (2004). It was used to determine whether an identified MJO event is primary or successive as defined by Matthew (2008).

a) Daily data from the global reanalysis ERA-Interim (Dee et. al. 2011). The horizontal resolution is 1.5° x 1.5°. The vertical resolutions are 25 hPa for 1000 hPa – 750 hPa, 50 hPa for 750 hPa – 250 hPa, and 25 hPa for 250 hPa – 100 hPa. Diabatic heating was estimated using the data as a residual of the thermodynamic equation following the approach of Yanai et al. (1973).

a) The ENSO index from Climate Predict Center, which is 3 month running mean of SST anomalies in the Niño 3.4 region based on Extended Reconstructed Sea Surface Temperature version 3b. A threshold of +/- 0.5K was used to define warm and cold ENSO events.

a) NOAA High-resolution Blended Analysis of daily sea surface temperature (SST) (Reynolds et al. 2007) with a horizontal resolution of 0.5° x 0.5°. The Indian Ocean Dipole (IOD) index (Saji et al. 1999) was calculated using the data smoothed by a 100-day running mean.

For a given variable, its long-term trend was first removed and then its annual climatology (all time mean for each calendar day) was removed from its daily time series to generate anomalies. A 7-day running mean was then applied to the anomalies to remove their high-frequency variability. The resulting anomalous time series are dominated by intra-seasonal variability.

3 Case selections

3.1 Convectively active episode

The RMM index (Wheeler and Hendon 2004) does not always accurately describe the location of active convection associated with the MJO, especially for individual events at their convective initiation stages over the Indian Ocean. The RMM index is based on global tropical coherent patterns of OLR and upper- and low-level zonal wind. Contributions from OLR are generally much less than the wind (Straub 2012). When MJO convection is weak or absent and convection-circulation coupling is feeble, such as prior to and during convective initiation of the MJO over the Indian Ocean, RMM phases are determined mainly by global-scale distributions of zonal wind instead of MJO convection over the tropical Indian Ocean. In these cases, the location and time of convective initiation of the MJO cannot be accurately determined by the RMM index. Other MJO indices based on global tropical patterns of convection (e.g., Matthews 2008) suffer from similar problems. To better describe MJO convective initiation over the Indian Ocean, we need local convective signals. The RMM index, however, provides reliable information of global wind perturbations of the MJO and can be used to distinguish MJO initiation over the Indian Ocean with and without circumnavigating propagation of previous MJO events, namely, the successive and primary MJO (Matthews 2008).

In this study, the anomalous precipitation time series of TRMM was used to define general convective variability over the tropical Indian Ocean. Let P be anomalous TRMM precipitation averaged over the Indian Ocean of the deep tropics[1] (10°S -10°N, 60° - 90°E) and δ_P its standard deviation. A large-scale convective event over the tropical Indian Ocean was detected if $P \geq \delta_P$ lasted continuously for at least 3 days. The first day of $P \geq \delta_P$ was defined as the day of convective initiation (day 0).

3.2 MJO and non-MJO

MJO signals in precipitation were extracted from the TRMM data by using time-space Fourier transform following Wheeler and Kiladis (1999). Spectral coefficients in the eastward intra-seasonal (20 - 80 days) and large-scale (zonal wavenumber 1 - 10) band were used to reconstruct a time series of MJO precipitation. It should be pointed out that this method suffers from a known but often forgotten caveat: all eastward spectral power does not belong to eastward propagating perturbations. Only that incoherent with its westward counterparts does (Hayashi 1982). For precipitation, the eastward power within the MJO band is about four times greater than its corresponding westward power (Zhang 2005). The possibly maximum error of taking all eastward power of precipitation to represent the MJO would be overestimating the MJO strength by 25%. This calls for a refined spectral method of extracting MJO signals. We used the commonly practiced but somewhat flawed Wheeler and Kiladis (1999) method in this study for the ease of comparison to results from many others using the same method.

Once a convective episode was identified (section 3.a), the following steps were taken to determine whether it was part of convective initiation of the MJO (Fig. 1). First, averaged MJO precipitation

[1] Hereafter referred to as tropical Indian Ocean.

over 10˚S-10˚N ($\bar{P}$) was calculated. Second, a threshold of 1.45 mm day-1 was chosen as the noise level of $\bar{P}$. This value is the averaged standard deviation of $\bar{P}$ over the Indian Ocean and Maritime Continent (60 - 120˚E). Third, if (a) $\bar{P}$ was greater than 1.45 mm day^{-1} at day 0 at any longitude between 60 – 90˚E and (b) an area of $\bar{P}$ > 1.45 mm day^{-1} (within the thick black contour in Fig. 1a) extended eastward through 100°E (the eastern boundary of the Indian Ocean) in the following days, then an MJO event was declared. This is equivalent to the 1.45 mm day^{-1} contour extending eastward passing 100˚E on the Hovmöller diagram of $\bar{P}$. Examples of thus identified MJO events are given in Fig. 1a as cases C2 and C3. If one of the two criteria was not satisfied, no MJO initiation was identified over the Indian Ocean and the case was regarded as a non-MJO event (e.g., case C1 in Fig. 1a).

Because of the influence of Asian Summer Monsoon, boreal summer MJO events, with their northward propagation component, are more complicated than winter ones (Wang and Rui 1990; Li et al. 2001). To avoid this complication and make our analysis clean, boreal summer cases were not included in this study. Totally 23 MJO events and 13 non-MJO events were identified during October - April of 1998 - 2009.

There is another complication. Some events started very weak ($\bar{P}$ < 1.45 mm day^{-1}) over the Indian Ocean, but they intensified rapidly as they moved over the Maritime Continent and western Pacific, where their $\bar{P}$ became greater than 1.45 mm day^{-1}. These cases were classified as the non-MJO events over the Indian Ocean based on the procedure described earlier. However, conditions over the Indian Ocean may have influenced their subsequent development into MJO events. Including them in non-MJO composites may potentially produce misleading results. These events (four) were not included in this study.

3.3 Primary and successive MJO

Based on conditions prior to convective initiation of the MJO over the Indian Ocean, each MJO event can be classified as primary or successive (Matthews 2008). Signals of a preceding MJO event prior to a successive MJO event mainly exist in the circulation. They can be identified through the RMM index on its phase diagram as counter-clockwise rotation through phases 7, 8, 1 and into 2 and 3 with an amplitude greater than 1 (e.g., Fig. 1b, red curve before day 0 of C3). In contrast, a primary MJO event can be identified if the amplitude of the RMM index started less than 1 in phase 7, 8 or 1, and becomes greater than 1 as it rotates counter-clockwise from phases 2 and 3 onward to 4, 5, 6, and 7 (e.g., Fig. 1b, blue curve before day 0 of C2). Of the 23 MJO events, 10 (~ 43%) were thus identified as successive and 13 (~ 57%) as primary. The percentage of successive MJO events is different from that (60%) found by Matthews (2008). The discrepancy may come from different sources. We used a combination of the RMM index with an amplitude threshold of 1 (i.e., one standard deviation) and TRMM precipitation to define MJO events over the Indian Ocean for October – April during 1998 – 2009; Matthews (2008) used an OLR-based index with a threshold of 0.4 over the entire tropics for all seasons during 1974 – 2005.

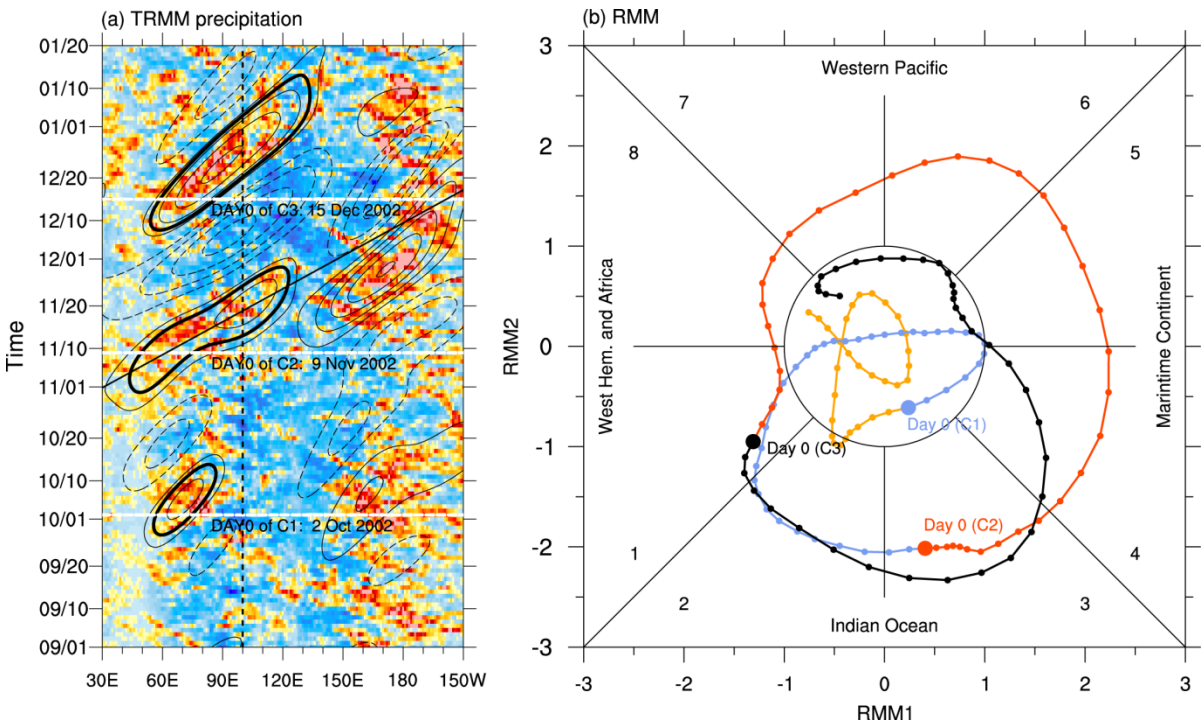

Figure 1 Three concecutive cases of convective initiation that led to a non-MJO event (Case C1), a primary MJO event (C2), and a successive MJO event (C3) during October – December 2002. (a) Hovmöllor diagrams of total (colors, mm day^{-1}) and MJO-filtered (contours, interval 1 mm day^{-1}) precipitation anomalies avergaged over 10°S – 10°N from Sep 1, 2002 to Jan 20, 2003. Dashed contours are for negative values, and zero contours omitted. Solid straight lines mark the 5 m s^{-1} eastward propagation speed. Day 0 is the day of convective initiation, and marked by the horizontal dashed white line. Thick contours enclose areas of precipitation > 1.45 mm/day. The vertical dotted line marks 100˚E. (b) RMM phase diagram. Each dot represents a day. Large blue, red, and black dots represent the day 0 for non-MJO, primary MJO, and successive MJO, respectively. The colors represent different time segments before, between, and after days 0.

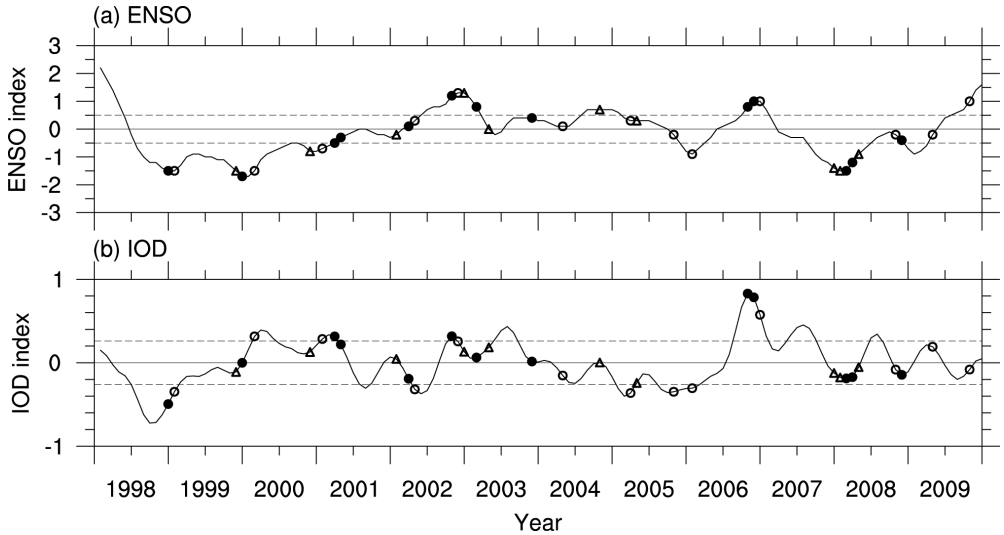

Figure 2 Time series of (a) the Nino 3.4 index (K) and (b) the Indian Ocean Diople index (K). Horizontal dashed lines mark ± 0.5K in (a) and ± one standard deviations in (b). Day 0 for each convectively active eposide is marked. Open circles are for the primary MJO, open triangles for the successvie MJO, and dots for non-MJO.

To examine possible modulation of convective initiation events of the MJO by ENSO and IOD, we show in Fig. 2 their timing relative to ENSO and IOD phases. These events sometimes cluster together but without any apparent connection to particular phases of ENSO and IOD. These events appear to be randomly distributed in all phases of ENSO. Influence of ENSO in the present study should therefore be minimal.

There might be signs of IOD influences. Successive MJO (triangles) occurred only in the neutral phase of IOD (within the two dashed lines). There were more primary MJO (open circles) in the negative phase (below the lower dashed line) than positive phase (above the upper dashed line). There are more non-MJO events (dots) in the positive than negative phases. This analysis period is, however, too short to establish any statistics for IOD modulations of the different types of convective events.

3.4 Verification

Our selection and classification procedures include subjective choices, although with physically based justifications. Their results need to be scrutinized. In this subsection, we compare composites of the three types of convective events: the primary MJO, successive MJO, and non-MJO. Composite Hovmöller diagrams of precipitation anomalies averaged over 10°S -10°N for these three types of events are shown in Figure 3. Eastward propagating positive anomalies in precipitation 30-40 days before day 0 (convective initiation) of the successive MJO are clearly seen (Fig. 3b). They are absent before convective initiation of the primary MJO (Fig. 3a). Interestingly, eastward propagation of negative anomalies in precipitation appears 10-20 days before day 0 of both primary and successive MJOs, but signals of statistical significance are very limited for the primary MJO. There is no eastward propagation signal for the non-MJO. But there are negative precipitation anomalies over the Indian Ocean before day 0, suggesting a local intra-seasonal stationary oscillation.

The general distinction between the two types of the MJO and non-MJO is also clearly displayed by their composites of the RMM index (Fig. 4). The amplitude of the RMM index is always smaller than 1 for the non-MJO (blue curve) but larger than 1 for the MJO over the Indian Ocean and part of the Maritime Continent (phases 2 – 4) after their convective initiation (day 0). The RMM index of the successive MJO (black) maintains its amplitude greater than 1 in phases 6 to 1 before convective initiation over the Indian Ocean (phase 1), whereas for the primary MJO (red) its amplitude starts close to zero at day -20 and then qucikly intensified to be greater than 1 after day -5 over the Indian Ocean (phase 2) and beyond. The inability of the RMM index in accurately identifying convective initiation of the MJO is also illustrated in Figure 4. Positive anomalies in precipiation of both primray and successive MJO reach their maxima at 85˚E at day 4 (Figs. 3a and b). But day 4 is in RMM phase 3 for the primary MJO and phase 2 for the successive MJO.

For both non-MJO and primary MJO, there is no obvious precursor in precipitation before its positive anomalies reach maxima and start to show different behaviors in zonal propagation. The rest of this article is focused on differences in preconditions for convective initiation between the primary MJO (hereafter simply referred to as the MJO) and non-MJO events. It is equally interesting to see what distinguishes MJO events that lead to successive events from those that do not. We leave this to another study.

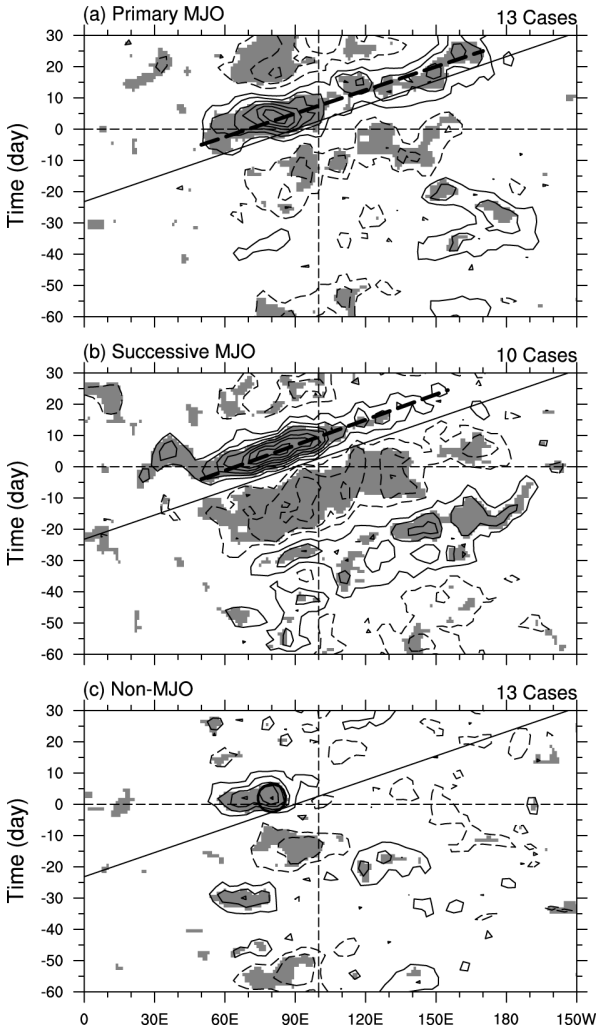

Figure 3 Composite Hovmöller diagrams of precipitation anamalies (contours, interval 1 mm day^{-1}) avergaged over 10°S – 10°N for (a) primary MJO events, (b) successive MJO events, and (c) non-MJO events. Dashed contours are for negative values, zero contours omitted. Results passing a student-t test at the 95% confidence level are shaded. Thin straight solid lines mark the 5 m s^{-1} eastward propagation speed. Thick straight dashed lines mark the central path of eastward propagation of positive anomalies. Thick circles mark the maximum centers for non-MJO. Vertical straight dashed lines mark 100°E.

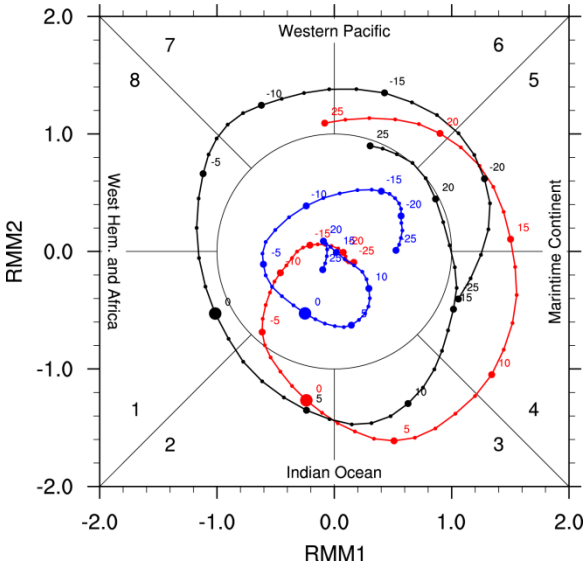

Figure 4 Composite of the RMM index for the (red) primary MJO, (black) successive MJO, and (blue) non-MJO. Each dot represents a day. Day 0 is marked by a large dot.

3.5 Composite

Composites were made for the 13 (primary) MJO events and 13 non-MJO events selected by the procedure described earlier in this section. All fields used for the composite are anomalies as described in section 2. A Student-t test was performed to identify results that are significant at the 95% confidence level. When discussing the composites, we will focus mostly on the significant results. However, all results with or without statistical significance will be presented together to provide a continuous spatiotemporal context for the significant results.

4 Results

In this section special attention is given to signals prior to convective initiation (day 0) and to precursors that may distinguish the MJO from non-MJO events before and during their convective development. The eastward propagating nature of the MJO and its absence in non-MJO events are evident not only in precipitation (Fig. 3) but also in many other fields shown in Fig. 5. A useful exercise of inspecting this and other time-longitude Hovmöller diagrams would be to block its upper portion (after day 0) and view only the lower portion (before day 0) to appreciate the difference, if any, in large-scale conditions prior to convective initiation between the MJO and non-MJO composites.

As early as 20 - 25 days prior to its convective initiation, eastward propagating signals of the MJO start over the central-western Indian Ocean in negative anomalies of 850 hPa zonal wind (Fig. 5a) and 400 hPa temperature (Fig. 5e). No such early eastward propagating signal exists with statistical significance in the non-MJO composites (Figs. 5b and f). Interestingly, there is westward propagation in 400 hPa temperatures of the non-MJO 10 days before its convective initiation (Fig. 5f). There are also obvious westward propagation signals in 500 hPa potential vorticity (PV) for both the MJO and non-MJO immediately after their convective initiation (Figs. 5g and h), suggesting the presence of equatorial Rossby waves. SST appears to be higher over a broader area of the Indian Ocean prior to convective initiation of the MJO than non-MJO, but signals with statistical significance are limited

(Fig. 5i). There are significant negative anomalies of SST near 100˚E in the non-MJO composite from 10 days before to 10 days after the convective initiation. There is no obvious difference between the MJO and non-MJO in PV at 500 hPa and moisture convergence at 850 hPa (Figs. 5c and d) or in the lower troposphere (850 – 500 hPa, not shown) before their convective initiation.

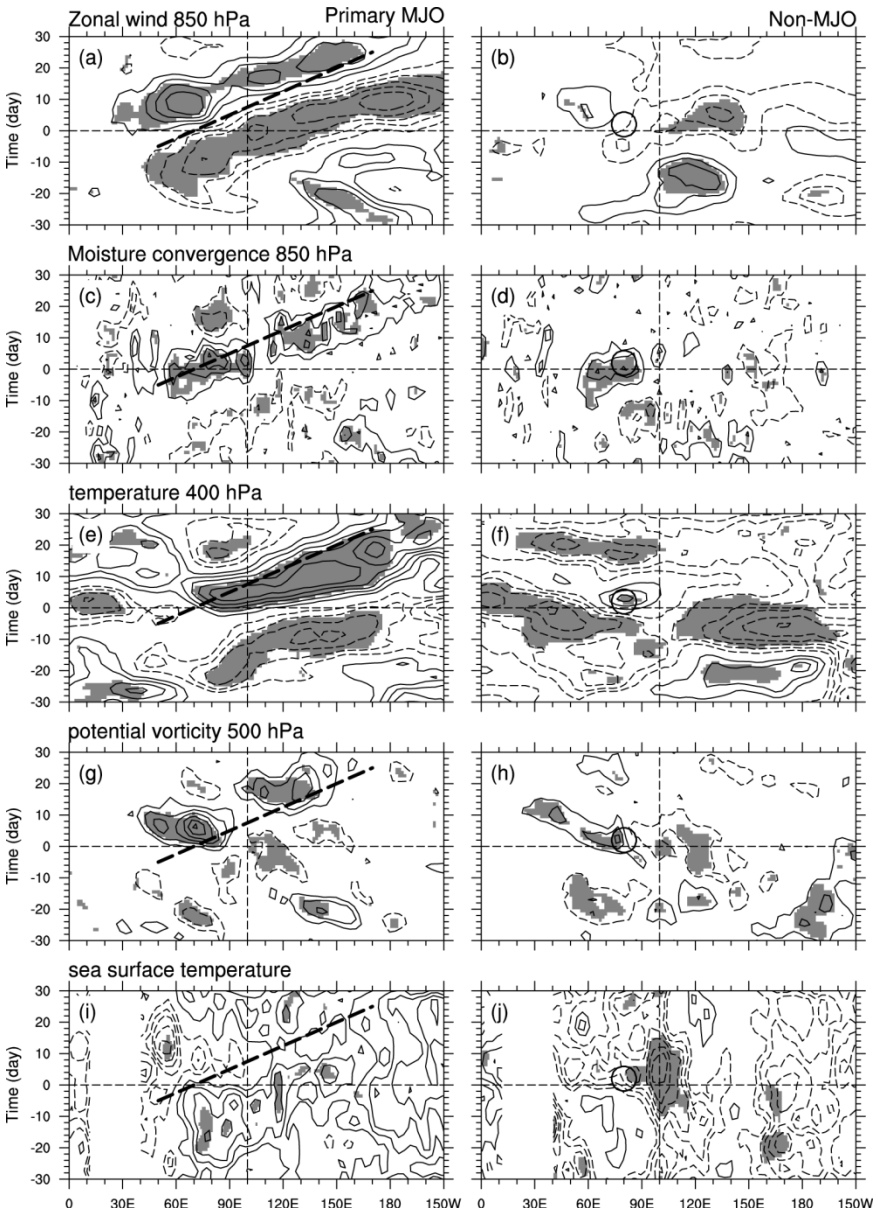

Figure 5 Composite Hovmöller diagrams of (from top to bottom) zonal wind at 850 hPa (interval 0.5 m s^{-1}), moisture convergence at 850 hPa (interval 3×10^{-9} Kg Kg^{-1} s^{-1}), temperature at 400 hPa (interval 0.1 K), potential vorticity at 500 hPa (interval 0.01PVU), and sea surface temperature (interval 0.05 K) averaged over 10˚S-10˚N for the (left column) MJO and (right) non-MJO. Dashed contours for negative values, zero contours omitted. Results passing the significance test at the 95% confidence level are shaded. Dark straight dashed lines mark the central path of eastward propagation of positive precipitation anomalies for the primary MJO in Figure 2a. Thick circles mark the maximum precipitation center for non-MJO in Fig. 2c.

4.1 Low-level wind

The eastward propagation of low-level easterly anomalies emerging over the tropical Indian Ocean 20 days before convective initiaiton of the MJO is one of the features that clearly distinguish the MJO from non-MJO convective events (Figs. 5a and b). This low-level easterly signal has been observed by Straub (2012). It can also be seen in the composite of 850 hPa wind based on the RMM index (phases 7 and 8 in Fig. 12 of CLIVAR 2009), where it coincides with eastward propagating negative anomalies in precipitation of the MJO from the Indian Ocean to the Maritime Continent. However, the RMM composite to a large degree describes the successive rather than primary MJO.

Composites of horizontal distributions of anomalies in precipitation and 850 hPa wind vectors for the (primary) MJO show easterlies over the equatorial western Indian Ocean on day -15 when most of the tropial Indian Ocean and Maritime Continent are covered by negative anomalies in precipitation (Fig. 6a). As time progresses, the easterlies extend northward as well as eastward (Figs. 6c and e). By day -6, they have reached the Maritime Continent (Fig. 6g). Up to this point, there is hardly any significant positive anomaly in precipitation over the equatorial Indian Ocean and there is hardly eastward propagation of the negative anomalies in precipitation, in contrast to the RMM composite (Fig. 12 of CLIVAR 2009). A positive anomaly in precipitation then quickly develops over the central equatorial Indian Ocean (day 0, Fig. 6k), which is accompanied by strengthened and widened easterlies over the Maritime Continent and emergence of equatorial westerlies over the western Indian Ocean (Fig. 6m). Both are part of the MJO circulation pattern associated with MJO convection as depicted by Madden and Julian (1972). In the non-MJO composite (Fig. 6, right column), significant low-level easterlies are absent over the tropical Indian Ocean until positive anomalies in precipitation appear near convective initiation (day -3).

The difference in zonal winds between the MJO and non-MJO is not only in the timing of their easterlies (much earlier for the MJO), but also in their latitudinal and vertical extent (Fig. 7). Easterlies extend from the surface to the mid troposphere, and from 15˚S to 10˚N for the MJO. They are more confined in space for the non-MJO events.

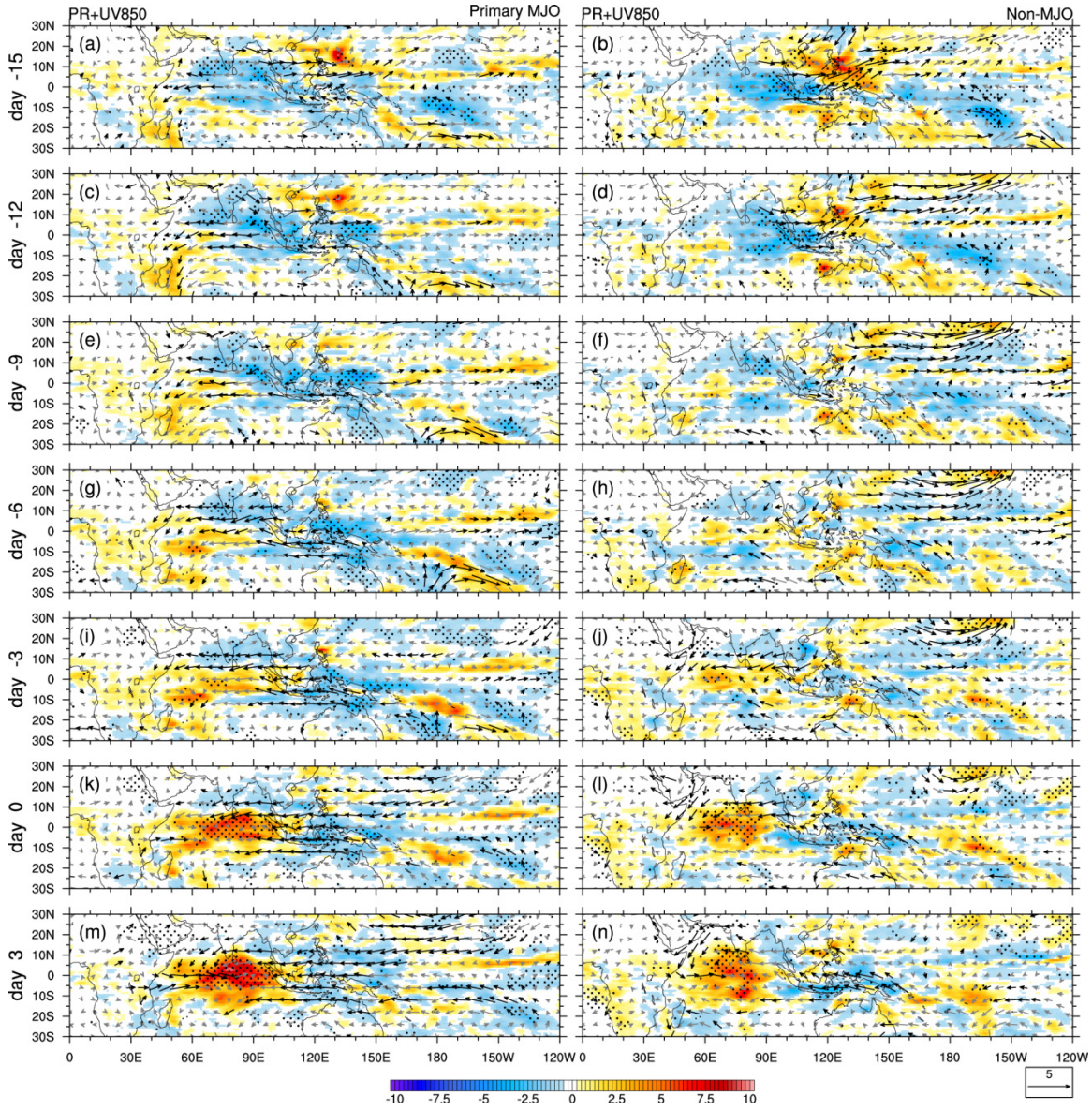

Figure 6 Three-day mean composites of anomalies in precipitation (colors, mm day^{-1}) and 850 hPa wind vectors (m s^{-1}) for the (left column) MJO and (right) non-MJO. Results passing the significance test at the 95% confidence level are stippled for precipitation and marked by black vectors for wind.

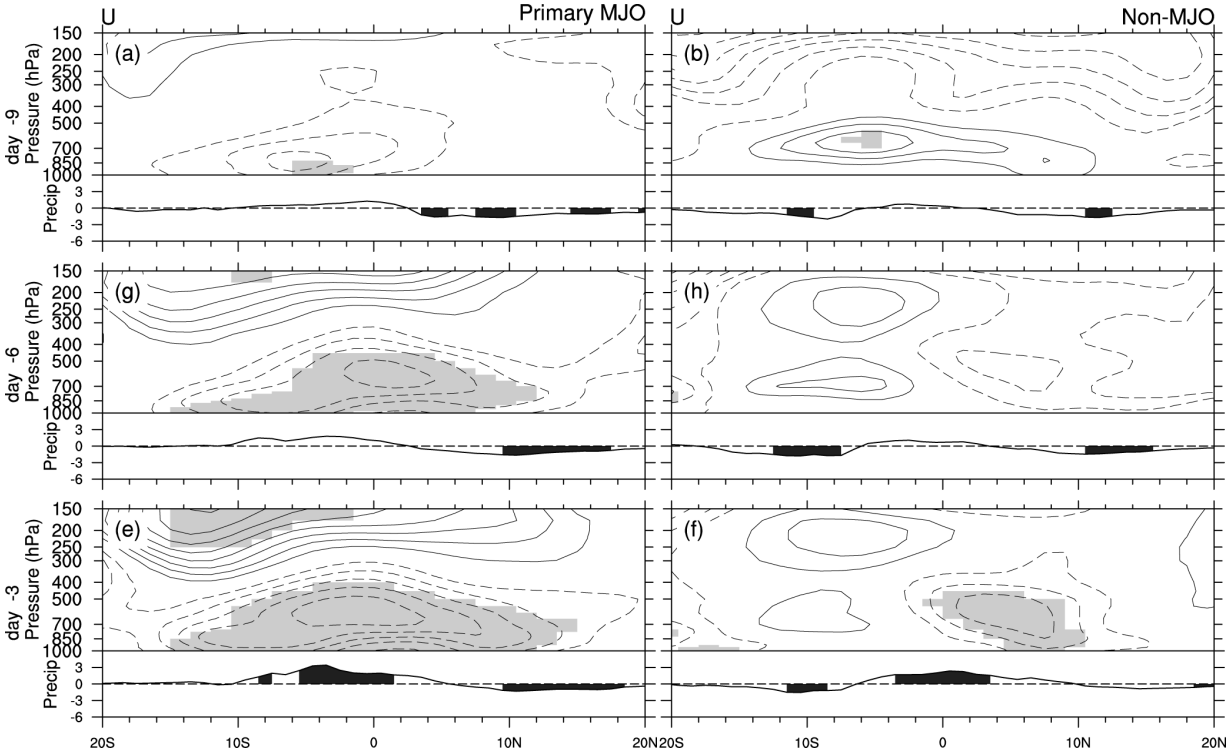

Figure 7 Three-day mean composites of zonal wind (interval 0.5 m s^{-1})averaged over 90 – 120˚E with coresponding precipitation (mm day^{-1}) averaged over 60 – 90˚E for the MJO (left column) and non-MJO (right). Results passing the significance test at the 95% confidence level are shaded for zonal wind and filled for precipitation.

4.2 Surface pressure

There are two possible reasons for the low-level easterly anomalies discussed in the previous subsection. One is anomalies in the zonal pressure gradient. The other is anomalous momentum transport from extratropics, upper levels, and/or flows of other scales. Only the first possibility is discussed here. Intraseasonal anomalies in pressure (geopotential height) do not change sign vertically from the surface to 5 km (from 1000 to 500 hPa) in the tropics. Their signals are strongest near the surface. We use surface pressure (SP) anomalies as a proxy of lower-tropospheric pressure anomalies.

For the MJO, there is a zonal wavenumber one structure in equatorial SP anomalies (Fig. 8, left column). About 20 days before the convective initiation, negative SP anomalies are over the longitudes of South America, Atlantic, and Africa, and positive SP anomalies are over the rest of the tropics. There is an equatorial low pressure surge penetrating from Africa eastward into the Indian Ocean (Fig. 8c). This low pressure surge quickly covers the entire equatorial Indian Ocean (Figs. 8e, g, i) and advances further to the Maritime Continent (Figs. 8k, m) and the western Pacific (Fig. 8o). By the time of the convective initiation over the Indian Ocean, this low pressure surge has reached the eastern Pacific (Fig. 8q). The average eastward propagation speed of the low pressure surge is around

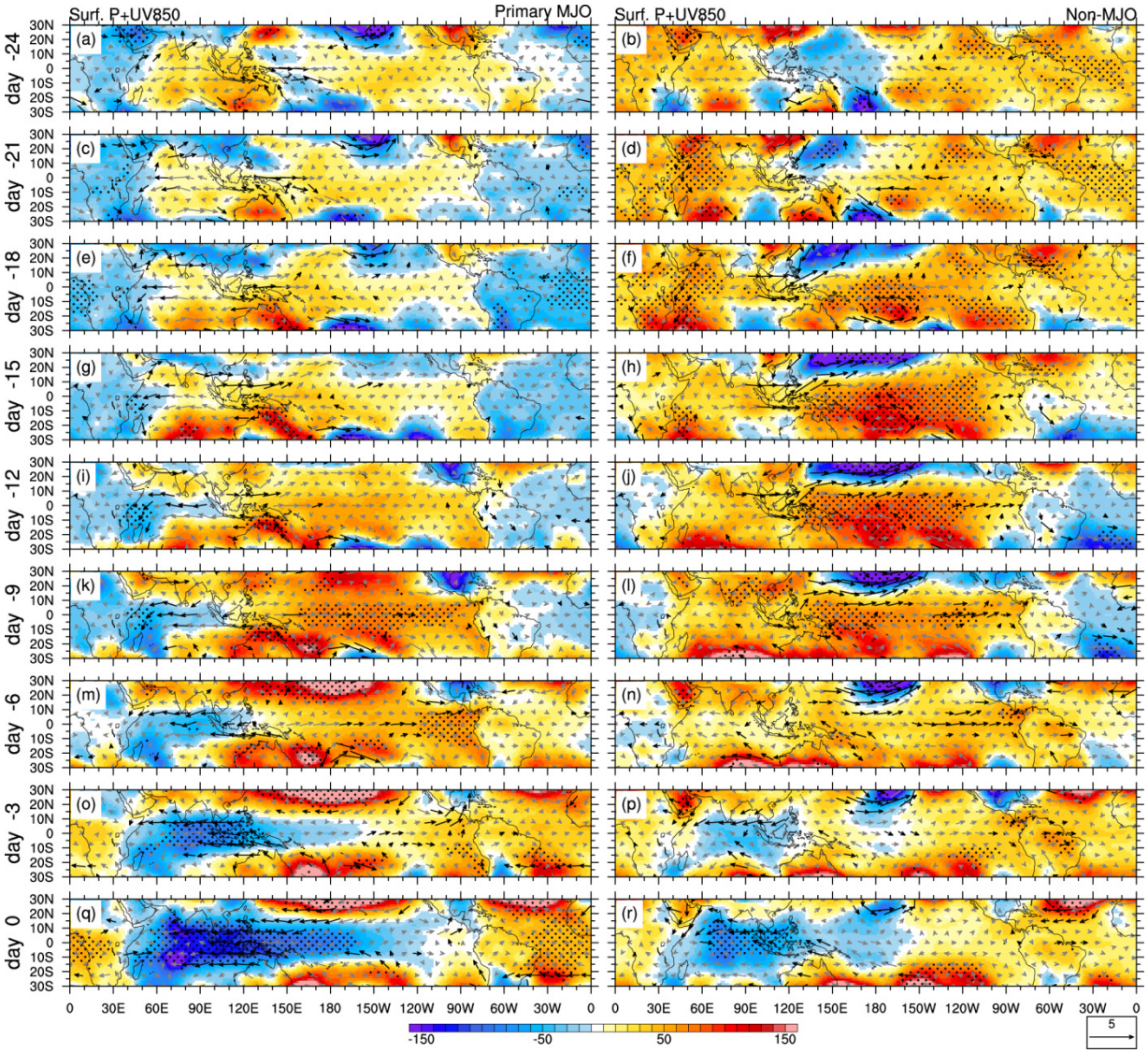

Figure 8 Same as Figure 6 but for anomalies in surface pressure (colors, Pa) and 850 hPa wind vectors (m s^{-1}).

5 m s^{-1} over the Indian Ocean and Maritime Continent before the convective initiation (days -21 to -6), and accelerates to 27.5 m s^{-1} after convection emerges over the Indian Ocean (days -6 to 0). Meanwhile, the eastern edge of the region with positive SP anomalies over the western coast of South America moves eastward from day -12 and reaches the eastern coast of Africa at the convective initiation day, with an average propagation speed of around 11 m s^{-1}. Such zonal wavenumber one structure in SP anomalies, the equatorial low pressure surge, and the eastward propagation of SP anomalies are all missing in the non-MJO composite (Fig. 8, right column), where SP anomalies appear to change sign locally.

The earliest appearance of the low-level easterly anomalies over the western equatorial Indian Ocean is cross the boundary between negative SP anomalies to the west and positive anomalies to the east about 18 – 15 days before the convective initiation (Figs. 8e and g). As the low pressure surge reaches the Maritime Continent, the low-level easterly anomalies are enhanced there (day -6). The

strengthening and widening of the equatorial low-level easterly anomalies (days -3 and 0) is more direcly related to the developing convection over the Indian Ocean than the low pressure surge.

It should be pointed out that signals of the low pressure surge are not always statistically significant. But they are robust in a sense that they become significant in a composite based on data of a longer record (see section 5).

4.3 Temperature

Matthews (2008) showed in his composite of the primary MJO negative temperature anomalies in the mid troposphere propagating both westward and eastward from the eastern Indian Ocean and Maritime Contiment 15 days prior to convective initiation. He interpreted the westward propagating negative temperature anomalies as a destabilizing factor for convective initiation of the primary MJO. In the present composite of the (primary) MJO, there are also signals of both westward and eastward propagation of negative temperature anomalies at 400 hPa over the Indian Ocean starting 20 days prior to convective initiation, but only the eastward propagating signals are significant (Fig. 5e). Significant westward propagation in negative temperautre anomalies is found in the non-MJO composite starting 10 days before its convective initiation (Fig. 5f). The presence and absence of the eastward propagating signals in negative temperature anomalies prior to convective initiaiton are another main distinction between the MJO and non-MJO events.

The negative temperature anomalies start at 400 hPa over the central Indian Ocean and gradually expand vertically and zonally as they move eastward (Fig. 9, left column). Their eastward propagating speed is about 5 ms^{-1} over the Indian Ocean and slightly faster over the Maritime Continent and the western Pacific. The average speed is about 6.5 ms^{-1} (determined by the moving speed of the trailing or western edge of the significant part of the anomalies). If clear sky radiative cooling caused negative temperature anomalies, it could hardly explain their vertical and zonal expansion and eastward propagation. The eastward propagating negative temperature anomalies before convection initiation of the non-MJO composite (Fig. 9, right column) are ambiguous, if exist at all.

In the MJO composite, there are anomalous westerlies and subsidence coinciding with the negative temperature anomalies. Negative precipitation anomalies are found underneath the negative temperature anomalies. Positive precipitation anomalies starts on day -6 at longitudes (~60˚E) without obvious tropospheric temperature anomalies. This suggests that the eastward propagating negative temperature anomalies do not trigger MJO convective initiation by destabilizing the atmosphere.

Once MJO convection is initiated, the tropospheric temperature responds quickly with positive anomalies centered at 300 hPa, flanked by negative anomalies above and to the west. This pattern is the same as observed by Kiladis et al. (2005) for the mature MJO. Meanwhile, the eastward propagating negative temperature anomalies continue moving eastward, albeit losing much of their significance.

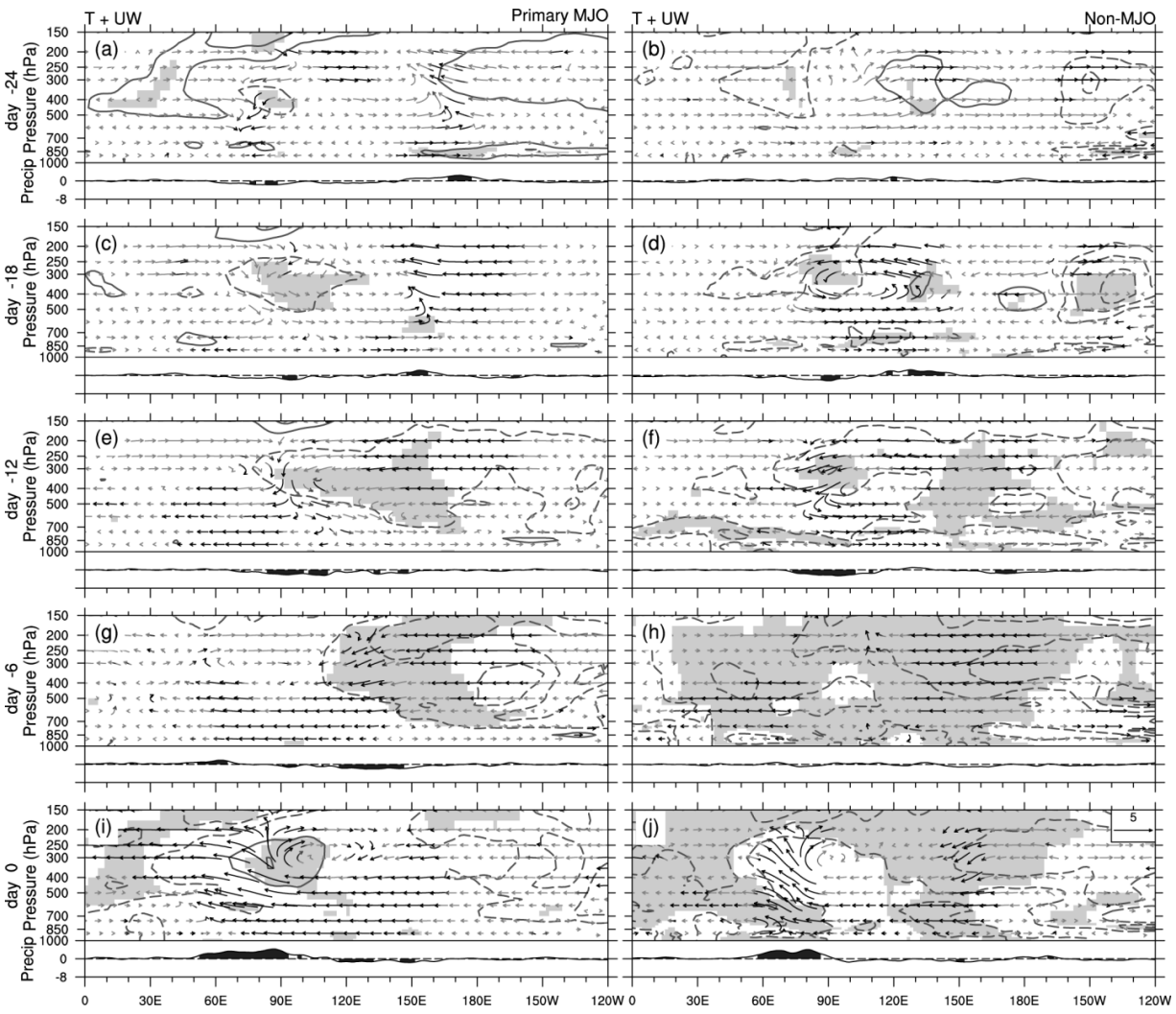

Figure 9 Three-day mean composites of anomalies in temperature (contours, interval 0.2 K), zonal-vertical circulation by zonal wind (m s^{-1}) and vertical velocity (Pa s^{-1}, scaled by 100), and precipitaion averaged over 10˚S-10˚N for the (left column) MJO and (right) non-MJO. Results passing the significance test at the 95% confidence level are shaded for temperature, highlighted by black vectors for wind, and filled for precipitation

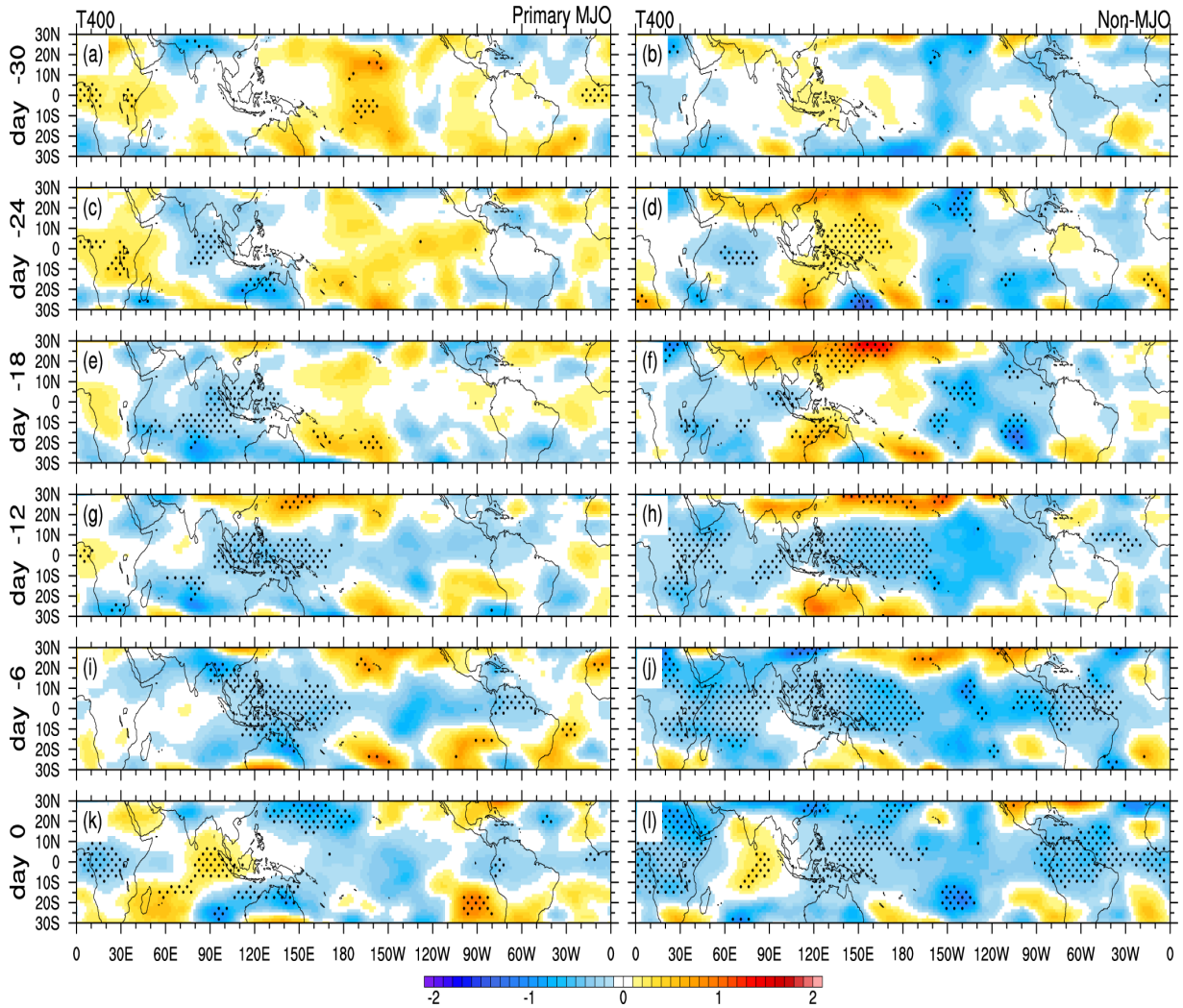

Figure 10 Same as Fig. 6 except for 400 hPa temperature anomalies (K) without wind vectors.

Horizontally, the negative temperature anomalies in the MJO composite are mostly confined to the tropics (Fig. 10, left column). They start over the tropical Indian Ocean, without much signs of being induced by extratropical or upstream perturbations. As positive precipitation anomalies emerge over the equatorial Indian Ocean immediately prior to convective initiation (day -6), the negative temperature anomalies exhibit a swallowtail pattern, with equatorial signals to the east and off-equatorial signals to the west. This is the same pattern that precipiation anomalies will develop into at a later time (Zhang and Ling 2012). No such a swallowtail pattern in temperature anomalies exists in the non-MJO composite (Fig. 10, right column).

4.4 Moisture

As mentioned earlier, there is no obvious difference in low-level moisture convergence between the MJO and non-MJO events prior to their convection initiation in the Hovmöller diagrams (Figs. 5c and d). There is a westward tilt in specific humidity (*q)* starting 6 days before and persisting through convective initiation of the MJO (Fig. 11, left column). This low-level moisture ahead (east of) MJO convection center has been observed by many previous studies (e.g., Johnson et al., 1999; Kemball-Cook et al., 2002; Kiladis et al., 2005). It appears to be related to the moisture flux by the low-level easterly anomalies. It also exists in the non-MJO composite (Fig. 11, right column), if less obviously.

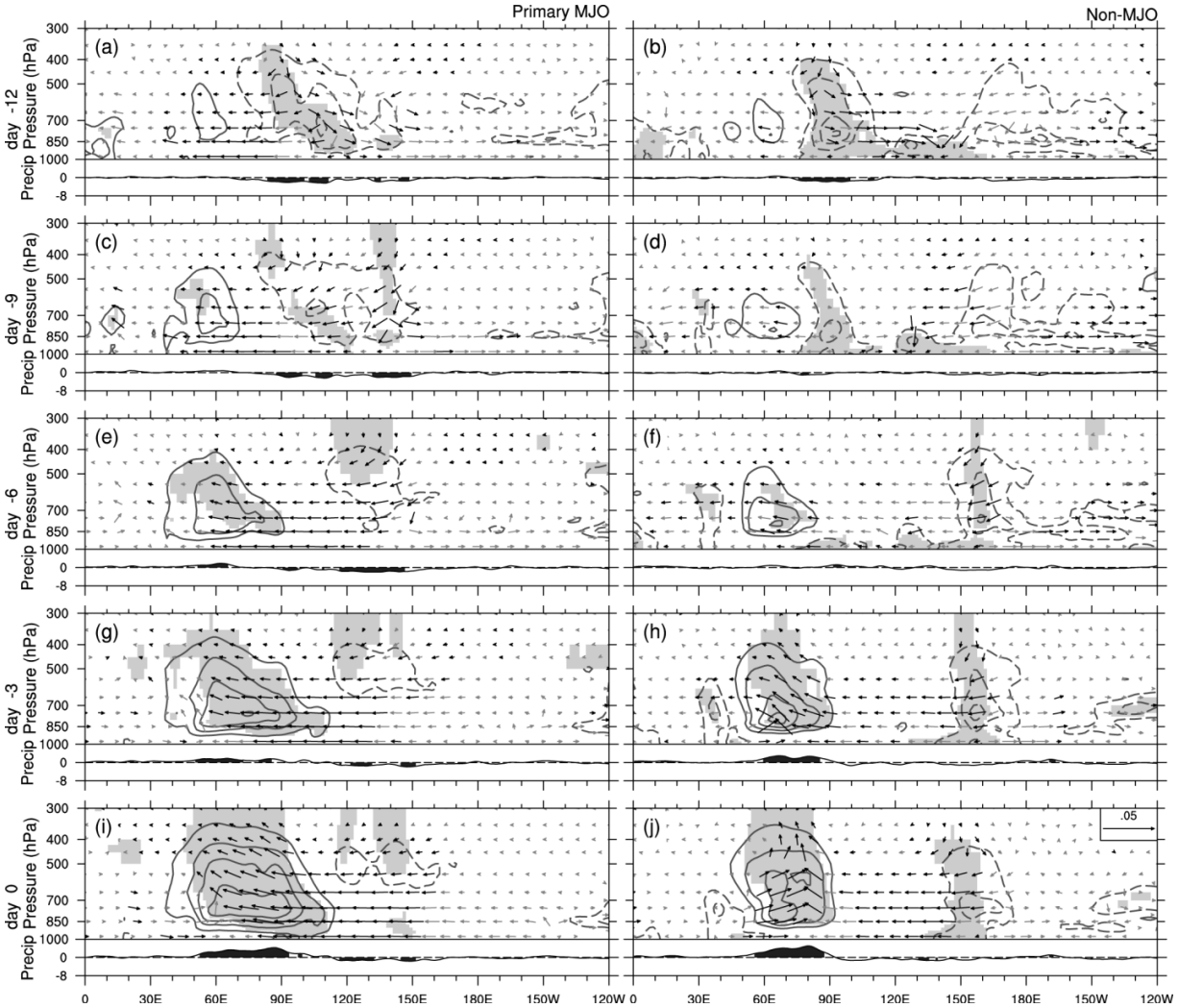

Figure 11 Same as Figure 9 except for specific humidity (q, contours, interval 0.2 g kg^{-1}) and moisture flux vectors of zonal (uq, m s^{-1} ×g kg^{-1}) and vertical (ωq, Pa s^{-1}×g kg^{-1}, scaled by 100) components.

4.5 Diabatic Heating

One interesting feature of diabatic heating associated with the MJO is its westward tilt (Lin et al. 2004; Kiladis et al. 2005; Jiang et al 2011; Ling and Zhang 2011). In the MJO composite (Fig. 12, left column), the westward tilt exists only in the lower troposphere. In the upper troposphere, there is an eastward tilt, which emerges three days before the convective initiation. These tilts make the diabatic heating of the MJO into a boomerang shape. To a lesser degree, this boomerang heating structure also exists in the non-MJO composite (Fig. 12, right column). The only obvious difference in diabatic heating between the MJO and non-MJO composites is the zonal scale of the heating, which is larger for the MJO than non-MJO.

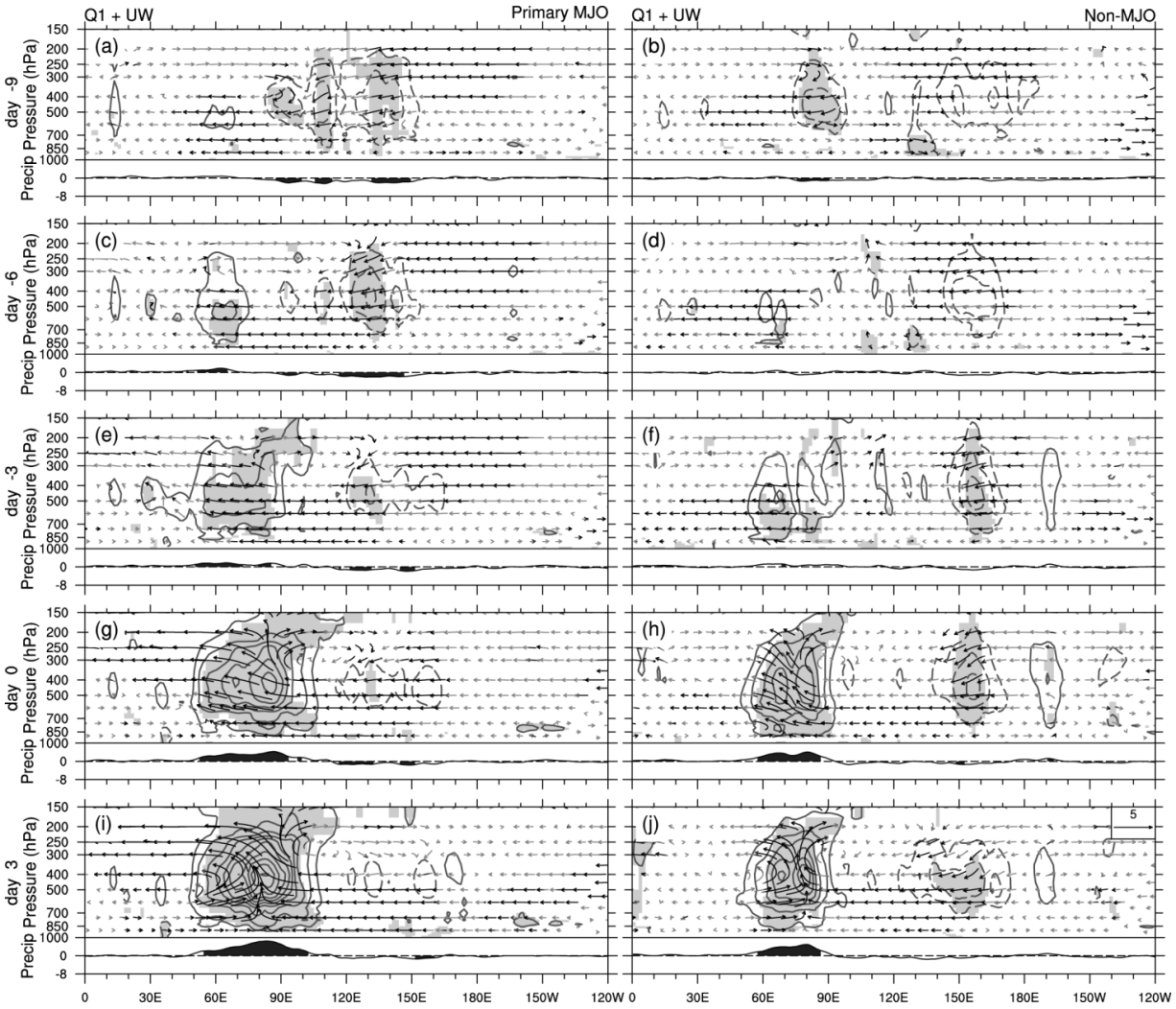

Figure 12 Same as Fig. 9 except for diabatic heating (contours, interval 0.3 K day^{-1}).

4.6 Potential vorticity

Composite Hovmöller diagrams of PV at 500 hPa, the peak level of tropospheric MJO PV, show tendencies of westward propagation of positive PV anomalies (Figs. 5g and h) starting on day 0 for the MJO and non-MJO both. This suggests the presence of equatorial Rossby waves (Wheeler and Kiladis 1999). There is no obvious difference over the Indian Ocean in PV between the MJO and non-MJO prior to day 0.

The only PV signal that distinguishes the MJO and non-MJO is the pair of cyclonic PV straddling the equator, a unique PV signature of the MJO (Zhang and Ling 2012). This PV pair is well established at convective initiation of the MJO and further strengthens afterward (Fig. 13, left column). It is generated by diabatic heating associated with the MJO in the tropics, with obvious connections to neither higher latitudes nor the stratosphere. A similar PV pair also emerges in the non-MJO composite (Fig. 13, right column) but its southern hemispheric part is weak and appears to connect with the extratropics.

4.7 Gross moist stability

The concept of gross moist stability (GMS) was introduced by Neelin and Held (1987) to measure the relationship between large-scale atmospheric flows and moist convection. It has been used to diagnose the MJO in model simulations (Sobel and Maloney 2012) as well as in observations (Haertel et al. 2008). Raymond et. al (2007) defined normalized GMS (NGMS) as the ratio of vertical integrated total divergence of moist entropy to vertical integrated horizontal moisture divergence.

Total NGMS and its horizontal and vertical components for the MJO and non-MJO as well as the corresponding precipitation anomalies, all averaged over 60° - 90°E and 10°S - 10°N, are compared in Fig. 14. Negative NGMS leading to convective initiation of the MJO has been documented (Raymond and Fuchs 2009; Hannah and Maloney 2011), but not found in this study. NGMS remains positive before and after convective initiation. It is larger than its October-April mean 10 – 15 days before convection initiation, starts to decrease as precipitation anomalies increase, reaches its minimum 4-5 days before the convective initiation but still positive, and gradually increases until after the time of precipitation maximum. The horizontal component is larger than the vertical one before day -5. The behavior of NGMS is of no difference for the MJO and non-MJO. This suggests that NGMS might be a useful diagnostic tool for convective development in the tropics but not unique for the MJO.

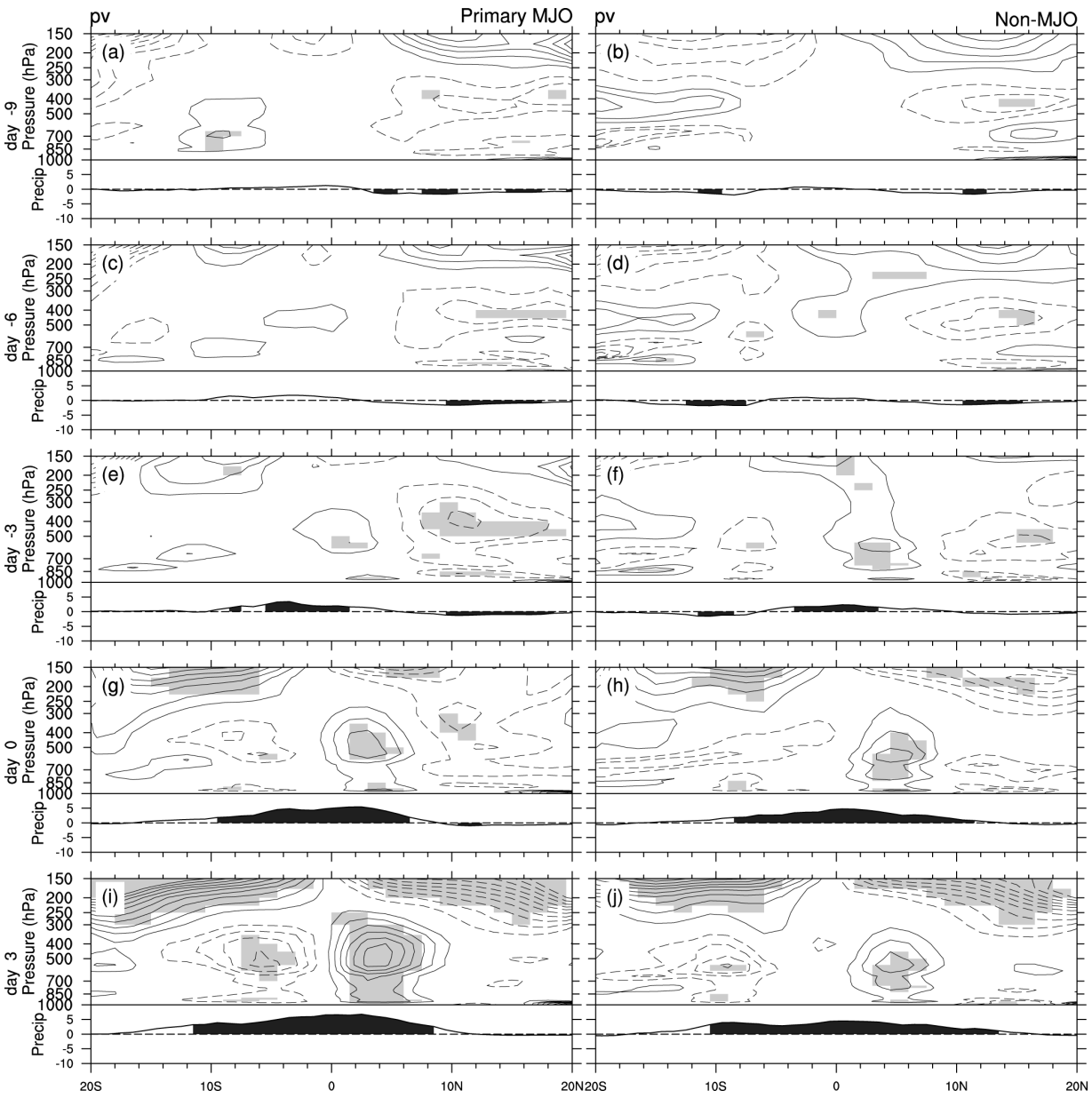

Figure 13 Three-day mean composites of anomalies in potential vorticity (contours, interval 0.01 PVU) and coresponding precipitation (mm day^{-1}) averaged over 60 - 90°E for the (left column) MJO and (right) non-MJO. Results passing the significance test at the 95% confidence level are shaded for potential vorticity and filled for precipitation.

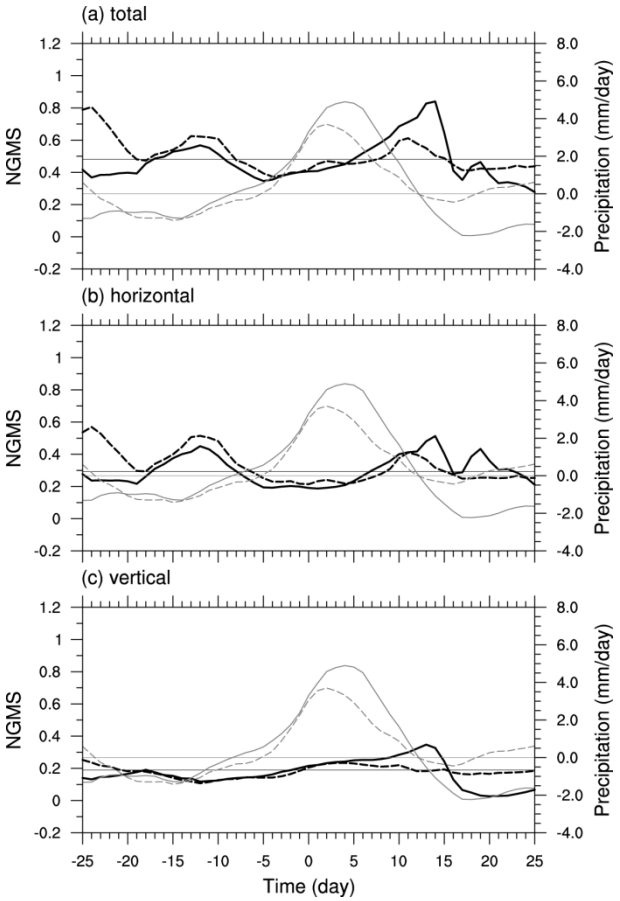

Figure 14 Composite of (a) normalized gross moist stability (NGMS) for the MJO (dark solid line) and non-MJO (dark dashed) and their (b) horizontal and (c) vertical components overlaid with their copresonding precipitation anomaly (grey lines), averaged over the tropical Indian Ocean (60 - 90°E and 10°S - 10°N). The horizontal lines mark the October – April mean of NGMS and precipitation.

5 Summary and Discussion

The purpose of this study is to seek precursors in large-scale fields that may distinguish events of convective initiation over the tropical Indian Ocean that lead to the MJO from those that do not. Such precursors may help us understand and predict convective initiation of the MJO. During October – April of 1998 – 2009, 36 large-scale convective events over the Indian Ocean were identified, out of which 13 primary MJO events and 13 non-MJO events were compared. Three most obvious and interesting precursor signals were found that are unique to the primary MJO. They all first emerge 10-20 days before convective initiation of the MJO, move eastward at a speed close to that of the MJO, while being absent or weak in non-MJO events. These signals are:

a) Lower-tropospheric (surface to 500 hPa) easterly anomalies. They start over the equatorial western Indian Ocean at low levels (850 hPa), extend upward into the entire lower troposphere and eastward to the rest of the Indian Ocean and the Maritime Continent, and expand over most tropical latitudes (Fig. 5a, left columns of Figs. 6 – 9). These easterly anomalies after the convective initiation become part of the canonical MJO circulation that is closely related to the eastward propagating convection center of the MJO as portrayed in the MJO schematic by Madden and Julian (1972). Their possible role in MJO initiation over the Indian Ocean might

be westward moisture transport from the Maritime Continent and generation of the low-level moisture convergence east of the developing convective center of the MJO (Fig. 11, left column). These eastward propagating low-level easterly anomalies before MJO initiation have been observed by Straub (2012).

a) Surface pressure (SP) anomalies. They represent pressure anomalies in the lower troposphere (surface – 5 km). They exhibit a zonal structure of wavenumber one. Negative SP anomalies first cover the longitudes from South America to Africa, and positive anomalies cover the rest of the tropics (Fig. 8, left column). An equatorial low pressure surge penetrates from Africa eastward through the Indian Ocean and Maritime Continent. Positive SP anomalies over the eastern Pacific also move eastward.

a) Negative temperature anomalies in the mid-upper troposphere (500 – 200 hPa). They start at 400 hPa over the Indian Ocean and immediately propagate eastward (Fig. 5e). They expand vertically and zonally but most of the time are confined to the equatorial region (Figs. 9 and 10, left columns). There is no obvious role of the negative temperature anomalies in convective initiation of the MJO. They were observed previously by Matthew (2008).

These three major signals that distinguish the MJO from non-MJO are confirmed by composites based on OLR data of 1980 – 2010. Other fields were also examined, but they do not clearly distinguish convective initiation of the MJO from that of non-MJO. Low-level moisture increases before convective initiation (Fig. 11). This precondition for deep convection, previously observed by many (e.g., Johnson et al., 1999; Kemball-Cook et al., 2002; Kiladis et al., 2005), is not unique to the MJO. Low-level diabatic heating starts before deep heating, resulting in a westward tilt that exists in both MJO and non-MJO only to a different extent (Fig. 12). The distinct structure of potential vorticity (PV) for the MJO emerges only during and after its convective initiation (Fig. 13). Warmer than normal sea surface temperature over the Indian Ocean appears to exist before convective initiation of the MJO but the significant signal is limited (Figs. 5i and j). For both MJO and non-MJO events, equatorial Rossby waves appear to exist (e.g., in PV) during the convective initiation, and normalized gross moist stability decreases when precipitation increases (Fig. 14) as theoretically predicted (Raymond and Fuchs 2009).

There are several shortcomings in this study. Its results are based on a single global reanalysis product. They need to be confirmed by other reanalysis products and, especially, by observations. We have focused on large-scale precursors between MJO and non-MJO convective initiation. But we did not explain why convection would occur in a large area in either case. We are not able to fully explain the three major signals that distinguish the MJO from non-MJO, namely, the low-level easterly anomalies, mid-upper tropospheric negative temperature anomalies, and surface pressure anomalies. Here, we can only offer some preliminary thoughts on them.

Matthew (2008) and Straub (2012) both suggested that a primary MJO event is preceded by global-scale perturbations, even though not by another MJO event. We agree. The three signals unique to the MJO do not show any obvious sign of extratropical, stratospheric, or upstream influences. We view them as intrinsically local to the tropospheric atmosphere over the tropical Indian Ocean. Although we did not make any effort to seek coherence between these three fields, we found their common features. They all appear 10 – 20 days before convective initiation of the MJO. They all propagate eastward at a

speed close to that of the MJO before its convective initiation. These made us ponder a possibility: There is a dry dynamic mode of the MJO.

The idea of a possible dry dynamic MJO mode is not new. Frederiksen and Frederiksen (1997) suggested that tropical intraseasonal oscillation might result from barotropical and baroclinic instability when the tropics and extratropics are coupled. Lin et al. (2007) extracted tropical intraseasonal, eastward propagating (16 m s^{-1}) signals in 250 hPa velocity potential and zonal wind from a dry global atmospheric model. They suggested that these signal in the dry model emerges as a response to extratropical influences. Wedi and Smolarkiewicz (2010) analytically and numerically tested a hypothesis that the core dynamics of the MJO is a weak nonlinear dry Rossby wave. Under favorable conditions (e.g., a zonal mean meridional shear of the zonal flow, extratropical influences), the nonlinear Rossby wave exhibits a solitary wave structure, persists at planetary scales, and moves slowly eastward (5.7 ms^{-1}).

The eastward propagating low-level easterlies anomalies, surface low pressure anomalies, and mid-upper tropospheric negative temperature anomalies observed in this study do not provide direct evidence for these previous hypotheses but support their general spirit. If a dry dynamic mode of the MJO exists in any form, these anomalies might be part of its signatures. MJO initiation would then be a process of supplying energy to its dynamic mode. There could be various sources of such energy supply, including but not limited to convection-circulation coupling, upstream and extratropical influences, scale interaction, and stochastic forcing. When active convection occurs in a large area without a proper receptor of an MJO dynamic mode, no MJO would be initiated.

Acknowledgments

Three anonymous reviewers provided careful comments on the submitted manuscript. Jian Ling thanks Anton Beljaars, Peter Bauer, and Frederic Vitart for hosting his visit to ECMWF. This study was support by NSF Grant AGS-1062202. The online availability of the ERA-Interim products, TRMM rainfall data, ENSO index, SST and MJO RMM index is highly appreciated.

References

Blade, I. and D. L. Hartmann, 1993: Tropical intraseasonal oscillations in a simple nonlinear model. *J. Atmos. Sci.*, **50,** 2922-2939.

CLIVAR, 2009: MJO Simulation Diagnostics. *J. Climate*, **22,** 3006-3030.

Dee, D. P. *and Coauthors*, 2011: The ERA-Interim reanalysis: configuration and performance of the data assimilation system. *Q. J. Roy. Meteor. Soc.*, **137,** 553-597.

Frederiksen, J. and C. Frederiksen, 1997: Mechanisms of the formation of intraseasonal oscillations and Australian monsoon disturbances: The roles of convection, barotropic and baroclinic instability. *Contrib. Atmos. Phys.*, **70,** 39-56.

Haertel, P. T., G. N. Kiladis, A. Denno, and T. M. Rickenbach, 2008: Vertical-mode decompositions of 2-day waves and the Madden-Julian oscillation. *J. Atmos. Sci.*, **65,** 813-833.

Hannah, W. M. and E. D. Maloney, 2011: The role of moisture-convection feedbacks in simulating the Madden-Julian oscillation. *J. Climate*, **24,** 2754-2770.

Hayashi, Y., 1982: Space-Time Spectral-Analysis and Its Applications to Atmospheric Waves. *J. Meteor. Soc. Japan*, **60,** 156-171.

Hendon, H., 1988: A simple model of the 40-50 day oscillation. *J. Atmos. Sci.*, **45,** 569-584.

Hsu, H. H., B. J. Hoskins, and F. F. Jin, 1990: The 1985/86 Intraseasonal Oscillation and the Role of the Extratropics. *J. Atmos. Sci.*, **47,** 823-839.

Huffman, G. J. *and Coauthors*, 2007: The TRMM multisatellite precipitation analysis (TMPA): Quasi-global, multiyear, combined-sensor precipitation estimates at fine scales. *J. Hydrometeorol.*, **8,** 38-55.

Jiang, X. *and Coauthors*, 2011: Vertical Diabatic Heating Structure of the MJO: Intercomparison between Recent Reanalyses and TRMM Estimates. *Mon. Wea. Rev.,* **139**, 3208–3223.

Johnson, R. H., T. M. Rickenbach, S. A. Rutledge, P. E. Ciesielski, and W. H. Schubert, 1999: Trimodal characteristics of tropical convection. *J. Climate*, **12,** 2397-2418.

Kemball-Cook, S., B. Wang, and X. H. Fu, 2002: Simulation of the intraseasonal oscillation in the ECHAM-4 model: The impact of coupling with an ocean model. *J. Atmos. Sci.*, **59,** 1433-1453.

Kemball-Cook, S. R. and B. C. Weare, 2001: The onset of convection in the Madden-Julian oscillation. *J. Climate*, **14,** 780-793.

Kiladis, G. N., K. H. Straub, and P. T. Haertel, 2005: Zonal and vertical structure of the Madden-Julian oscillation. *J. Atmos. Sci.*, **62,** 2790-2809.

Kim, H. M., C. D. Hoyos, P. J. Webster, and I. S. Kang, 2010: Ocean-atmosphere coupling and the boreal winter MJO. *Clim. Dyn.*, **35,** 771-784.

Knutson, T. R. and K. M. Weickmann, 1987: 30-60 Day Atmospheric Oscillations - Composite Life-Cycles of Convection and Circulation Anomalies. *Mon. Wea. Rev.*, **115,** 1407-1436.

Knutson, T. R., K. M. Weickmann, and J. E. Kutzbach, 1986: Global-Scale Intraseasonal Oscillations of Outgoing Longwave Radiation and 250-Mb Zonal Wind during Northern-Hemisphere Summer. *Mon. Wea. Rev.*, **114,** 605-623.

Kummerow, C. *and Coauthors*, 2000: The status of the Tropical Rainfall Measuring Mission (TRMM) after two years in orbit. *J. Appl. Meteor.*, **39,** 1965-1982.

Lau, K. M. and L. Peng, 1987: Origin of Low-Frequency (Intraseasonal) Oscillations in the Tropical Atmosphere .1. Basic Theory. *J. Atmos. Sci.*, **44,** 950-972.

Li, C. Y., Z. X. Long, and Q. Y. Zhang, 2001: Strong/weak summer monsoon activity over the South China Sea and atmospheric intraseasonal oscillation. *Adv. Atmos. Sci.*, **18,** 1146-1160.

Lin, H., G. Brunet, and J. Derome, 2007: Intraseasonal variability in a dry atmospheric model. *J. Atmos. Sci.*, **64,** 2422-2441.

Lin, J. L., B. Mapes, M. H. Zhang, and M. Newman, 2004: Stratiform precipitation, vertical heating profiles, and the Madden-Julian oscillation. *J. Atmos. Sci.*, **61,** 296-309.

Ling, J. and C. D. Zhang, 2011: Structural Evolution in Heating Profiles of the MJO in Global Reanalyses and TRMM Retrievals. *J. Climate*, **24,** 825-842.

Madden, R. A. and P. R. Julian, 1971: Detection of a 40-50 Day Oscillation in Zonal Wind in Tropical Pacific. *J. Atmos. Sci.*, **28,** 702-708.

Madden, R. A. and P. R. Julian, 1972: Description of Global-Scale Circulation Cells in Tropics with a 40-50 Day Period. *J. Atmos. Sci.*, **29,** 1109-1123.

Matthews, A. J., 2008: Primary and successive events in the Madden-Julian Oscillation. *Q. J. Roy Meteor Soc*, **134,** 439-453.

Neelin, J. D. and I. M. Held, 1987: Modeling Tropical Convergence Based on the Moist Static Energy Budget. *Mon. Wea. Rev.*, **115,** 3-12.

Neelin, J. D. and J. Y. Yu, 1994: Modes of Tropical Variability under Convective Adjustment and the Madden-Julian Oscillation .1. Analytical Theory. *J. Atmos. Sci.*, **51,** 1876-1894.

Ray, P. and C. Zhang, 2010: A case study of the mechanics of extratropical influence on the initiation of the Madden-Julian oscillation. *J. Atmos. Sci.*, **67,** 515-528.

Ray, P., C. Zhang, J. Dudhia, and S. S. Chen, 2009: A numerical case study on the initiation of the Madden-Julian Oscillation. *J. Atmos. Sci.*, **66,** 310-331.

Raymond, D. J. and Z. Fuchs, 2009: Moisture Modes and the Madden-Julian Oscillation. *J. Climate*, **22,** 3031-3046.

Raymond, D. J., S. L. Sessions, and Ž. Fuchs, 2007: A theory for the spinup of tropical depressions. *Q J Roy Meteor Soc*, **133,** 1743-1754.

Reynolds, R. W., T. M. Smith, C. Liu, D. B. Chelton, K. S. Casey, and M. G. Schlax, 2007: Daily high-resolution-blended analyses for sea surface temperature. *J. Climate*, **20,** 5473-5496.

Saji, N. H., B. N. Goswami, P. N. Vinayachandran, and T. Yamagata, 1999: A dipole mode in the tropical Indian Ocean. *Nature*, **401,** 360-363.

Seo, K. H. and A. Kumar, 2008: The onset and life span of the Madden–Julian oscillation. *Theoretical and Applied Climatology*, **94,** 13-24.

Seo, K. H. and E. J. Song, 2012: Initiation of Boreal Summer Intraseasonal Oscillation: Dynamic Contribution by Potential Vorticity. *Mon. Wea. Rev.*, **140,** 1748-1760.

Seo, K. H., W. Q. Wang, J. Gottschalck, Q. Zhang, J. K. E. Schemm, W. R. Higgins, and A. Kumar, 2009: Evaluation of MJO Forecast Skill from Several Statistical and Dynamical Forecast Models. *J. Climate*, **22,** 2372-2388.

Sobel, A. and E. Maloney, 2012: Moisture Modes and the Eastward Propagation of the MJO. *J. Atmos. Sci.*, **70,** 187-192.

Straub, K. H., 2012: MJO initiation in the Realtime Multivariate MJO index. *J. Climate*.

Wang, B. and H. Rui, 1990: Synoptic Climatology of Transient Tropical Intraseasonal Convection Anomalies - 1975-1985. *Meteorol. Atmo. Phys.*, **44,** 43-61.

Webber, B. G. M., A. J. Matthews, K. J. Heywood, and D. P. Stevens, 2012: Ocean Rossby waves as a triggering mechanism for primary Madden–Julian events. *Q J Roy Meteor Soc*., **138,** 514-527.

Wedi, N. P., and P. K. Smolarkiewicz, 2010: A nonlinear perspective on the dynamics of the MJO: Idealized large-eddy simulations. *J. Atmos. Sci.*, **67**, 1202–1217.

Wheeler, M. and G. N. Kiladis, 1999: Convectively coupled equatorial waves: Analysis of clouds and temperature in the wavenumber-frequency domain. *J. Atmos. Sci.*, **56,** 374-399.

Wheeler, M. C. and H. H. Hendon, 2004: An all-season real-time multivariate MJO index: Development of an index for monitoring and prediction. *Mon. Wea. Rev.*, **132,** 1917-1932.

Yanai, M., S. Esbensen, and J. H. Chu, 1973: Determination of Bulk Properties of Tropical Cloud Clusters from Large-Scale Heat and Moisture Budgets. *J. Atmos. Sci.*, **30,** 611-627.

Yu, J. Y. and J. D. Neelin, 1994: Modes of Tropical Variability under Convective Adjustment and the Madden-Julian Oscillation .2. Numerical Results. *J. Atmos. Sci.*, **51,** 1895-1914.

Zhang, C. D., 2005: Madden-Julian oscillation. *Rev. Geophys*, **43,** RG2003, doi: 10.1029/2004RG000158.

Zhang, C. D. and J. Ling, 2012: Potential Vorticity of the Madden-Julian Oscillation. *J. Atmos. Sci.*, **69,** 65-78.

Zhao, C., T. Li, T. Zhou, 2013: Precursor Signals and Processes Associated with MJO Initiation over the Tropical Indian Ocean. *J. Climate*, **26**, 291–307.